Journal of Materials Science & Technology 150 (2023) 233–244

Contents lists available at ScienceDirect

Journal of Materials Science & Technology

journal homepage: www.elsevier.com/locate/jmst

Research Article

Regulation of TiO_2 nanoarrays on titanium implants for enhanced osteogenic activity and immunomodulation

Ruoyu Li[a], Hongyu Zhang[b], Xiaohong Yao[a], Bin Tang[a,*], Paul K Chu[c], Xiangyu Zhang[a,d,*]

[a] Shanxi Key Laboratory of Biomedical Metal Materials, College of Materials Science and Engineering, Taiyuan University of Technology, Taiyuan 030024, China
[b] Department of Occupational Disease, Second Hospital of Shanxi Medical University, Taiyuan 030001, China
[c] Department of Physics, Department of Materials Science and Engineering, and Department of Biomedical Engineering, City University of Hong Kong, Tat Chee Avenue, Kowloon, Hong Kong, China
[d] College of Biomedical Engineering, Taiyuan University of Technology, Taiyuan 030024, China

ARTICLE INFO

Article history:
Received 28 October 2022
Revised 1 December 2022
Accepted 3 December 2022
Available online 10 February 2023

Keywords:
TiO_2 nanoarrays
Osteogenic activity
Immunomodulation
Hydrothermal treatment

ABSTRACT

The surface topography of implants plays a major role in osteogenesis and immunomodulation. In this study, three types of TiO_2 nanoarrays including nanorod arrays with a diameter of 45 nm (TiO_2-N), nanorod arrays with a diameter of 60 nm (TiO_2-N N), and nanocone arrays (TiO_2-NW) are prepared on titanium and the behavior of bone marrow stromal cells (BMSCs) and polarization of macrophages are studied. Compared to the planar titanium control, TiO_2 nanoarrays facilitate osteogenesis of BMSCs and stimulate the pro-healing M2 phenotype. However, adhesion, spreading, proliferation, and osteogenic differentiation of BMSCs are more pronounced on TiO_2-N N than both TiO_2-N and TiO_2-NW. TiO_2-NN also produces the best immune microenvironment, while TiO_2-NW is more favorable than TiO_2-NN from the viewpoint of cell adhesion and spreading of osteoblasts.

© 2023 Published by Elsevier Ltd on behalf of The editorial office of Journal of Materials Science & Technology.

1. Introduction

With the accelerating global trend of population aging and the increasing incidence of dental and orthopedic related diseases, there is a growing demand for implants [1]. Titanium (Ti) and its alloys have been widely used as artificial implant materials due to excellent mechanical properties, biocompatibility, and corrosion resistance [2–5]. However, the nanometer-thick oxide layer on the surface of Ti also renders Ti-based alloys biologically inert which makes stable osseointegration difficult [6–8]. Osseointegration is a complex bone and implant healing process, and the rapid establishment of strong and durable connections between implant and bone tissues is vital to osseointegration [9]. Therefore, enhancing the interface interaction between Ti and bone tissue is highly desirable [10].

Numerous studies have shown that the surface morphology of Ti implants can facilitate cell adhesion, spreading, proliferation and differentiation [11–17]. Yu et al. found that nanorods were favorable for endothelial cell adhesion and angiogenesis [18]. Yuan et al. prepared nanopores by sandblasting and acid etching and found the nanopores were conducive to osteoblast adhesion, proliferation and osteogenic differentiation [19]. Yang et al. believed that nanowebs prepared by electrochemical anodization were beneficial to stem cell adhesion and osteogenic differentiation [20]. Fabrication of the nanostructures on Ti by surface modification to enhance osteogenesis or angiogenesis is still the focus of current research.

The primary techniques currently used to improve the bioactivity and compatibility of Ti implants include acid etching, anodization, alkali heat treatment, sandblasting, electrochemical etching, hydrothermal treatment, and so on [21–26]. In particular, the hydrothermal technique which is simple, environmentally friendly, and economical [27] has been used to produce a variety of nanostructures such as nanorods, nanotubes, and nanopores with good biocompatibility [28–32]. Yao et al. have observed that nano-flakes prepared on Ti hydrothermally have excellent osteogenic ability [33]. Ma et al. have fabricated various nanostructures on Ti by the alkali heat treatment and found that the materials induce osteogenic differentiation of stem cells [34]. In our previous studies, TiO_2 nanorod arrays were hydrothermally prepared on Ti and proliferation, spreading and differentiation of osteoblasts were demonstrated [35–38]. However, the effects of various nanorod arrays on the osteogenic activity of stem cells and immunomodulation of macrophages have not been systematically studied.

* Corresponding authors.
E-mail addresses: tangbin@tyut.edu.cn (B. Tang), zhangxiangyu@tyut.edu.cn (X. Zhang).

https://doi.org/10.1016/j.jmst.2022.12.023
1005-0302/© 2023 Published by Elsevier Ltd on behalf of The editorial office of Journal of Materials Science & Technology.

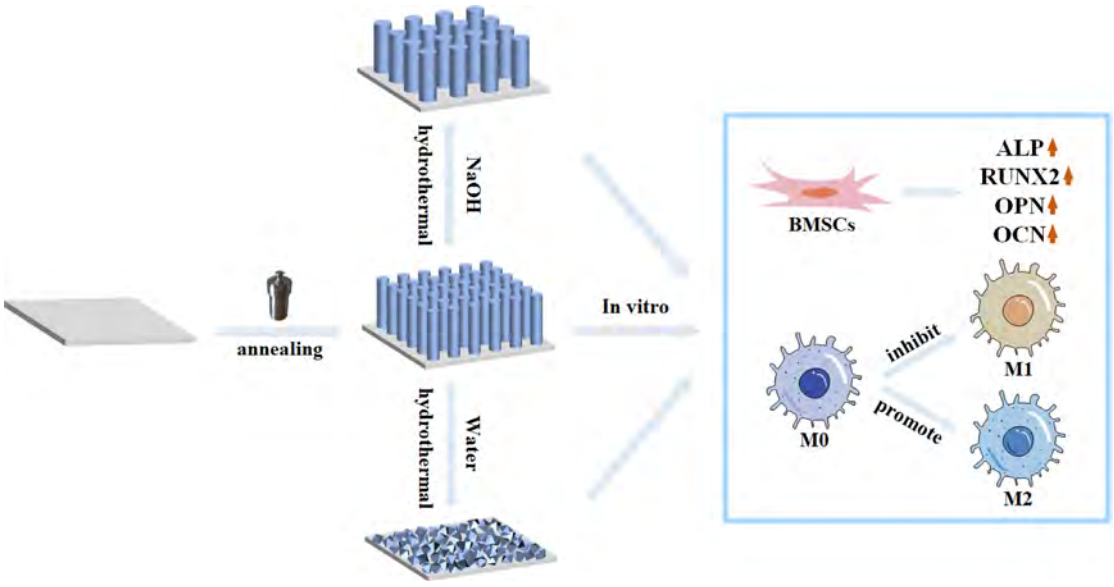

Fig. 1. Schematic illustration of the preparation of nanoarrays on Ti and its effect on osteogenesis and immunomodulation *in vitro*.

In this study, the TiO_2 nanorod array (TiO_2-N) prepared by a one-step hydrothermal treatment in NaOH undergoes a second hydrothermal treatment to form TiO_2 nanorods with a larger diameter (TiO_2-NN) and nanocones (TiO_2-NW) in NaOH and deionized water, respectively. The effects of the different surface morphologies of TiO_2-N, TiO_2-NN and TiO_2-NW on osteogenic activity and immunomodulation are studied systematically (Fig. 1).

2. Experimental section

2.1. Preparation of different nanoarrays on Ti

High-purity titanium (Ti) plates with an ASTM classification of Gr1 were cut into samples with dimensions of 3 cm × 3 cm × 2 mm and sonicated in acetone, ethanol and deionized water successively. The samples were placed in a 50 mL Teflon-lined stainless-steel autoclave containing 1 mol/L NaOH and hydrothermally treated at 220 °C for 4 h. Afterwards, the samples were sonicated in deionized water for 30 s and immersed in 0.5 mol/L HCl for 0.5 h. After annealing in a muffle furnace at 550 °C for 2 h, TiO_2-N was obtained. To prepare other morphologies, Ti was treated hydrothermally at 220 °C in 1 mol/L NaOH for 4 h and then underwent a second hydrothermal process at 220 °C for 4 h in a 50 ml Teflon-lined stainless-steel autoclave containing 1 mol/L NaOH solution and deionized water, respectively. After soaking in 0.5 mol/L HCl for 0.5 h and annealing at 550 °C for 2 h, TiO_2-NN and TiO_2-NW were obtained, respectively.

2.2. Characterization

Field-emission scanning electron microscopy (FE-SEM, Ultra55, Zeiss, Germany) and transmission electron microscopy (TEM, Tecnai G20, FEI, USA) were used to observe the surface morphology and microstructure. The surface composition was determined by X-ray photoelectron spectroscopy (XPS, K-Alpha, Thermo Fisher Scientific). The phase composition was determined by X-ray diffraction (XRD, Rigaku Dmax-3C, Cu K_α radiation, 2θ from 5° to 90°, step size of 0.02°). The roughness of the samples was examined by atomic force microscopy (AFM, XE-100, Park Systems) and the surface contact angles were measured on a contact angle meter (JC2000D2, Powereach, China) at room temperature by the sessile drop method.

2.3. Protein adsorption

1 mL of the minimum essential medium alpha medium (α-MEM, Gibco, America) containing 10% fetal bovine serum (FBS, Sijiqing, China) was introduced onto each sample placed on a 24-well plate. After incubation for 4 h, the medium was removed. The samples were washed with the phosphate buffer (PBS) and agitated in the 1% sodium dodecyl sulfate (SDS) solution for 1 h to collect the protein. The protein adsorbed by the samples was assayed by the enhanced BCA kit (cat# P0009; Beyotime).

2.4. Bone marrow stromal cells

2.4.1. Cell culture

According to the common protocol [39], bone marrow stromal cells (BMSCs) were extracted from the tibiae and femur of 3-week-old rats (generations 2 to 4) were used in the study. The cells were cultured with the α-MEM medium containing 1% streptomycin, 1% penicillin, and 10% FBS at 37 °C in an incubator filled with 95% air and 5% CO_2. The BMSCs were incubated on the samples with a cell density of 1×10^4 cells/cm^2 and the medium was changed once a day.

Additional 10 mmol/L β-glycerophosphate (Ekear, China), 50 μg/mL ascorbic acid (Ekear, China) and 10 nmol/L dexamethasone (Ekear, China) were added to the osteogenic medium to prepare the osteogenic induction medium for the experiments on osteogenic induction.

2.4.2. Cell adhesion and skeleton

The cells were incubated on the samples for 1, 4, and 8 h. After washing with PBS, the cells were fixed with 4% paraformaldehyde (PFA) for 40 min and stained with 4,6-diamidino-2-phenylindole (DAPI, Sigma, USA) in the dark for 10 min. Subsequently, fluorescent images were captured under a confocal laser scanning electron microscope (CLSM, C2 Plus, Nikon).

Prior to the morphological observation, the cells were cultured on the samples for 24 h. They were washed with PBS and fixed with 4% PFA for 40 min. Fluorescein isothiocyanate (FITC, Sigma, USA) was added and the cells were stained in the dark for 1 h, followed by counterstaining with DAPI for 10 min in darkness. Finally, fluorescent images were acquired randomly by CLSM.

2.4.3. Live/dead staining

The viability of cells on the samples was determined by live/dead fluorescent staining (calcein AM and EthD-1). The cells were seeded and washed with PBS after incubation for 1, 3, and 5 days. 50 μL of the staining solution was dropped onto the samples and incubated in the dark for 1 h. The live cells (green) and dead cells (red) were observed by CLSM.

2.4.4. Cell proliferation

Cell proliferation was quantified by the 3-(4,5-dimethylthiazol-2-yl)−2,5-diphenyltetrazolium bromide (MTT, Sigma, USA) assay. The cells were cultured and incubated for 1, 3 and 5 days. At each time point, the samples were rinsed thrice with PBS and transferred to a new 24-well plate. 900 μL of the α-MEM medium and 100 μL of the MTT solution were added to each well and incubated in the dark for 4 h. The mixture was removed and the crystals were dissolved with 1 mL of dimethyl sulfoxide (DMSO, Sigma, USA). The optical density (OD) of the solution was measured by a microplate reader (Infinite F50, TECAN) at 492 nm.

2.4.5. Cell morphology

The morphology of the BMSCs on the samples was observed by FE-SEM. The cells were seeded, incubated for 24 h, fixed with 3% glutaraldehyde, and dehydrated with gradient alcohol. After drying and gold plating, spreading of the BMSCs was monitored by FE-SEM.

2.4.6. Alkaline phosphatase (ALP) activity

After stimulation in osteogenic induction medium for 4 and 7 days, the cells were rinsed gently with PBS, fixed with 4% PFA, stained with the ALP color development kit (cat#C3206; Beyotime, China) for 30 min, and imaged under an inverted light microscope (Zeiss). The cells were lysed in the cell lysis solution (cat#P0013j; Beyotime) and the ALP activity of the BMSCs was determined using the ALP detection kit (cat#P0321; Beyotime, China).

2.4.7. Collagen secretion

The direct red (Sigma, America) stain was used to quantify type I collagen secretion from the cells. The cells were seeded and induced by the osteogenic induction medium for 7 and 14 days. Thereafter, the samples were washed with PBS, fixed by 4% PFA, and stained with direct red in the aqueous saturated picric acid (0.1 wt.%) for 18 h. After rinsing with 0.1 mol/L acetic acid, the cells were decolorized with 1 mL of the fading solution (0.2 mol/L NaOH/methanol 1:1) and the OD value was measured at 570 nm on a microplate reader.

2.4.8. Extracellular matrix (ECM) mineralization

Extracellular matrix mineralization was determined by alizarin red (Aladdin, China) staining. After the cells were grown in the osteoinductive medium for 7 and 14 days, the samples were rinsed three times with PBS and fixed in 75% ethanol for 1 h. The cells were then stained with 40 mmol/L alizarin red stain for 30 min and washed with deionized water until the water was clear. The cells were eluted with 500 μL of 10% cetylpyridinium chloride for 2 h and the OD value of the solution was determined at 570 nm on a microplate reader.

2.4.9. Osteogenesis-related gene expression

To further investigate the effects of the surface nanostructures on the expression of osteogenesis-related genes in the BMSCs, the cells were collected after culturing for 5 days. The RNA and reverse transcribed RNA were extracted by the Eastep® Super Total RNA Extraction Kit (Promega) and PrimeScript™ RT Kit (Takara), respectively. The expression levels of alkaline phosphatase (ALP), runt-related transcription factor 2 (RUNX2), osteopontin (OPN), and osteocalcin (OCN) were assayed by the StepOne Real-Time PCR System (Applied Biosystems) according to the manufacturer's protocols of TB Green Premix Ex Taq II (Takara). The gene content was determined by the comparative CT ($\Delta\Delta$CT) method and the gene expression of GAPDH was used for normalization. The primer sequences used in RT-qPCR are presented in Table 1.

Table 1
Primers for RT-PCR.

Genes	Primers	Sequences (5′-3′)
Homo	Forward	AGCCAACTCGTCACAGTCC
RUNX2	Reverse	ACATCGGTGATGGCAGGAAG
Homo	Forward	GACAAACTGGGGCCTGAGATA
ALP	Reverse	CTGACTTCCCTGCTTTCTTGG
Homo	Forward	ACTGATTTTCCCACGGACCT
OPN	Reverse	CTCCTCGCTTTCCATGTGTG
Homo	Forward	TCACACTCCTCGCCCTATTG
OCN	Reverse	AGCCAACTCGTCACAGTCC

2.5. Biocompatibility of osteoblasts in vitro

2.5.1. Cell culture

The *in vitro* cell experiments were performed on the osteoblasts (MC3T3-E1, Shanghai Chinese Academy of Sciences, Catalog number: GNM15). The experiments were performed by seeding 1 mL of cells (1×10^4 cells/cm^2) on the sample surface and the medium was changed once a day. The culturing method was the same as that shown in Section 2.4.1.

2.5.2. Cell adhesion and skeleton

The experimental protocol was the same as that described in Section 2.4.2.

2.5.3. Cytotoxicity

The experimental protocol was the same as that described in Section 2.4.3.

2.5.4. Cell proliferation

The experimental protocol was the same as that shown in Section 2.4.4.

2.6. Macrophages

2.6.1. Cell culture

The murine-derived macrophage cell line RAW 264.7 (TIB-71, ATCC, VA, USA) was used in this study. The cells were incubated in DMEM supplemented with 10% FBS and 1% (v/v) penicillin/streptomycin and placed in a cell culture incubator containing 5% CO_2. After culturing in the normal medium overnight, lipopolysaccharide (LPS, 100 ng/mL) was added to the culture medium for 6 h to activate the macrophages. The medium was replaced with serum-free normal medium.

2.6.2. Cell morphology

The morphology of the macrophages was observed by FE-SEM. The cells (2×10^4 cells/cm^2) were seeded on the sample surface, cultured in normal medium for 24 h, stimulated by LPS, and cultured in serum-free normal medium for 12 h. 2.5% glutaraldehyde was used to fix the cells and the morphology was examined by FE-SEM according to the method described in Section 2.4.5.

2.6.3. Immunofluorescence staining

The inducible nitric oxide synthase (iNOS, M1 marker) and cluster of differentiation 206 (CD206, M2 marker) were used as markers to assess the phenotype of the macrophages. The cells (5×10^4 cells/cm^2) were cultured and incubated in the normal medium for

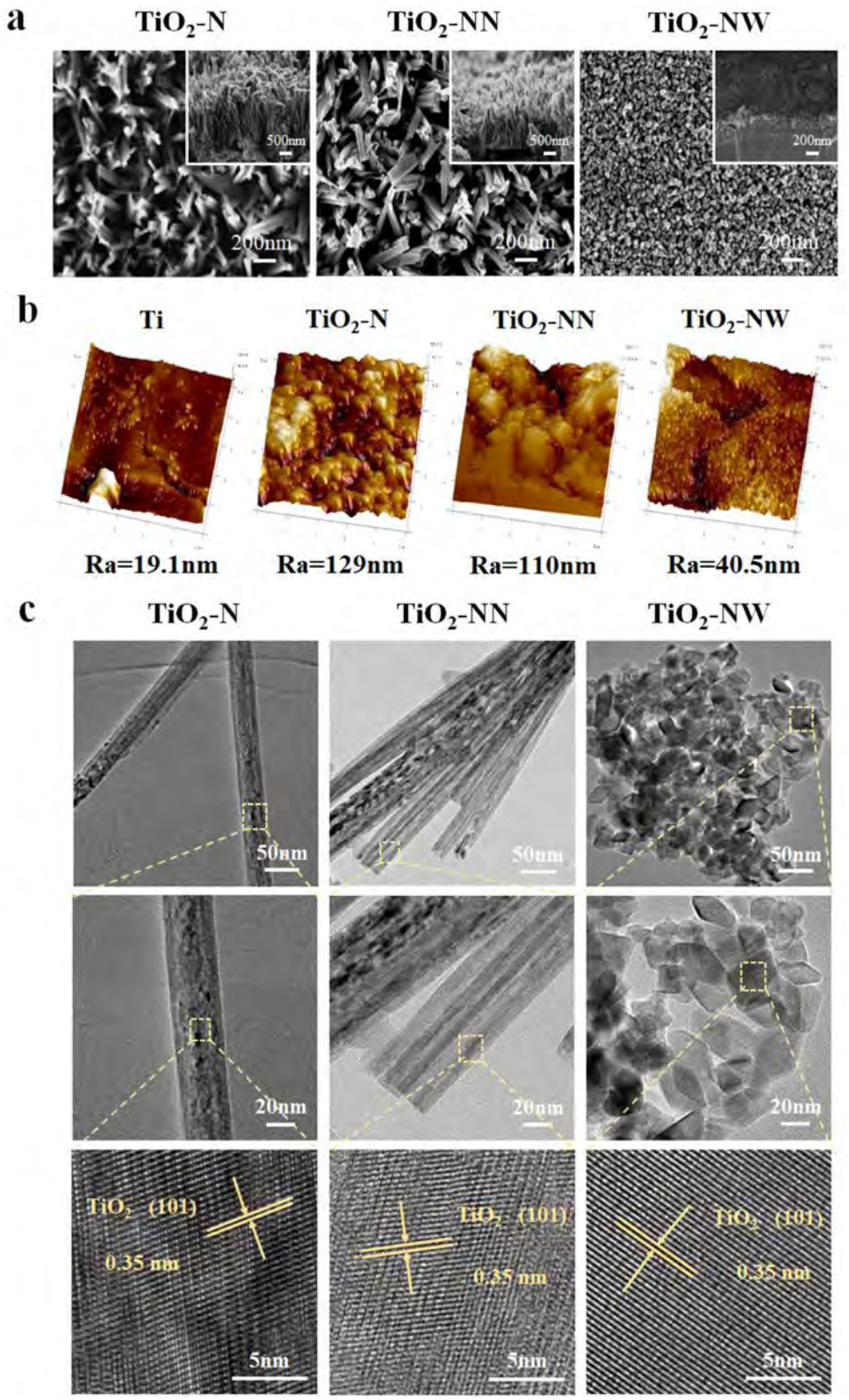

Fig. 2. (a) Surface and cross-sectional images of TiO_2-N, TiO_2-NN, and TiO_2-NW, (b) surface roughness of Ti and TiO_2 nanoarrays obtained by AFM, and (c) TEM images of TiO_2-N, TiO_2-NN, and TiO_2-NW.

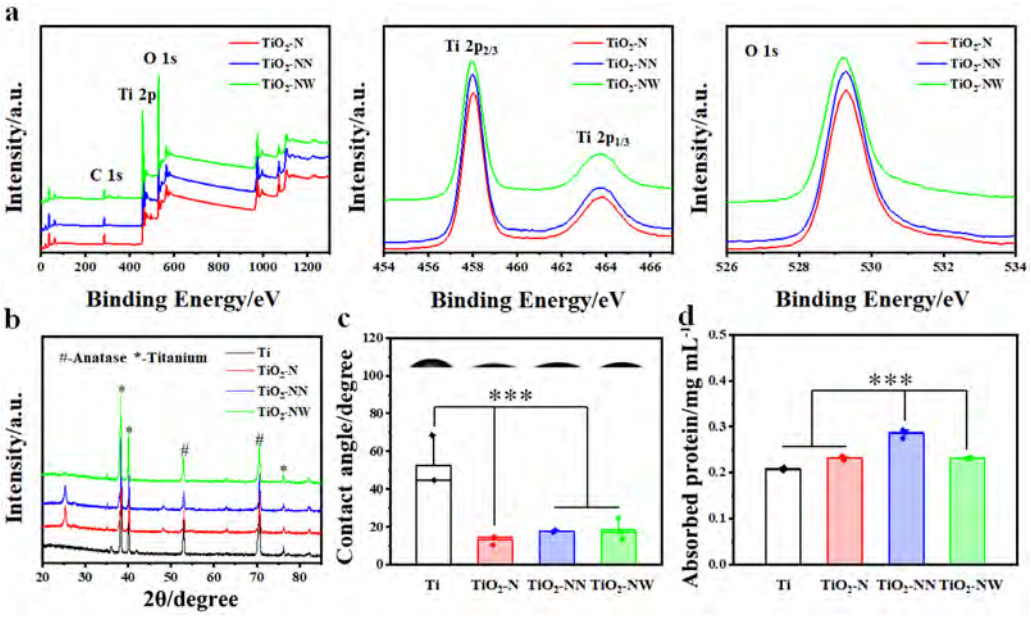

Fig. 3. (a) XPS survey spectra and high-resolution spectra of Ti 2p and O 1 s of the TiO_2 nanoarrays, (b) XRD patterns of Ti, TiO_2-N, TiO_2-NN, and TiO_2-NW, (c) surface wettability of Ti, TiO_2-N, TiO_2-NN, and TiO_2-NW, and (d) total adsorbed proteins on Ti, TiO_2-N, TiO_2-NN and TiO_2-NW after incubation for 4 h in the medium containing 10% α-DMEM ($^{***}p < 0.001$).

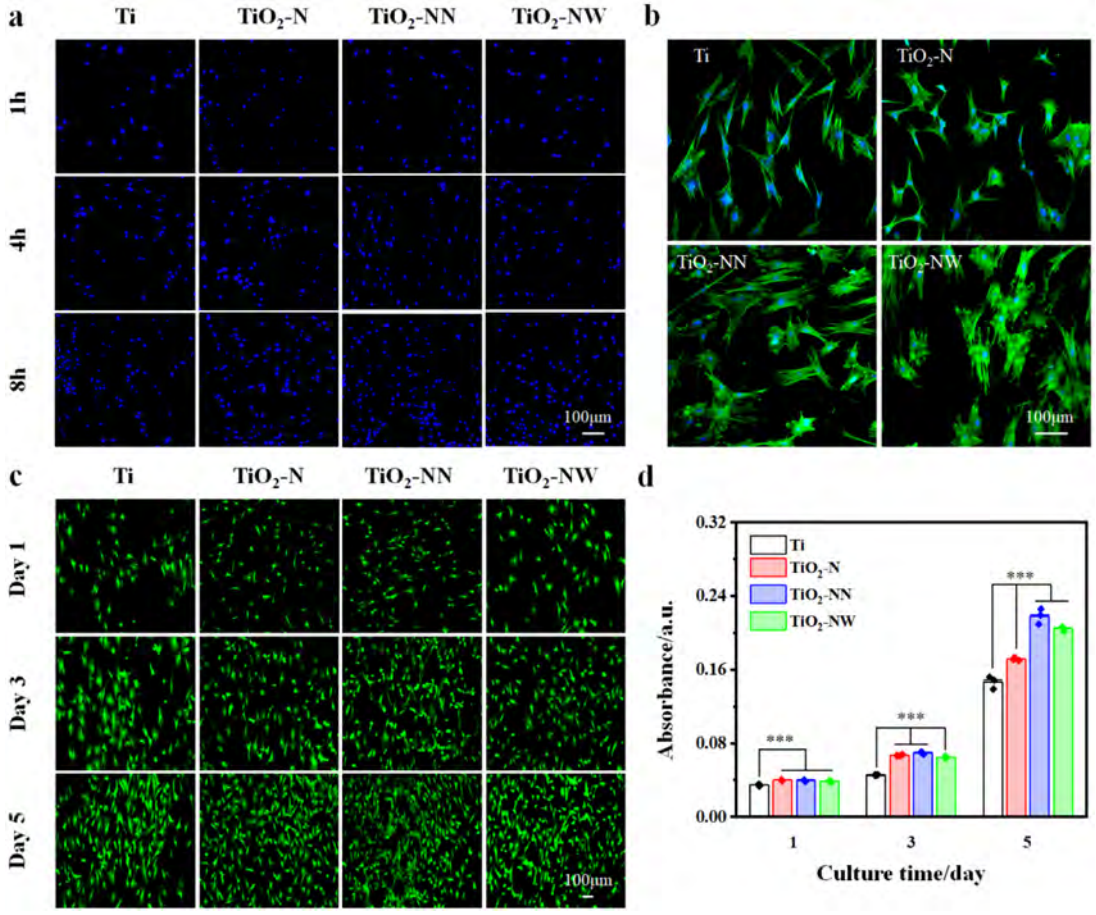

Fig. 4. Effects of the surface nanoarrays on osteogenic regulation of BMSCs. (a) CLSM images of the nuclei of the BMSCs on Ti, TiO_2-N, TiO_2-NN, and TiO_2-NW after culturing for 1, 4 and 8 h and (b) cytoskeleton of BMSCs. After culturing for 24 h, F-actin is stained with FITC (green) and the cell nuclei are stained with DAPI (blue). (c) CLSM images after live/dead staining of the BMSCs after culturing for 1, 3, and 5 days and (d) MTT results of the BMSCs after 1, 3 and 5 days ($^{***}p < 0.001$).

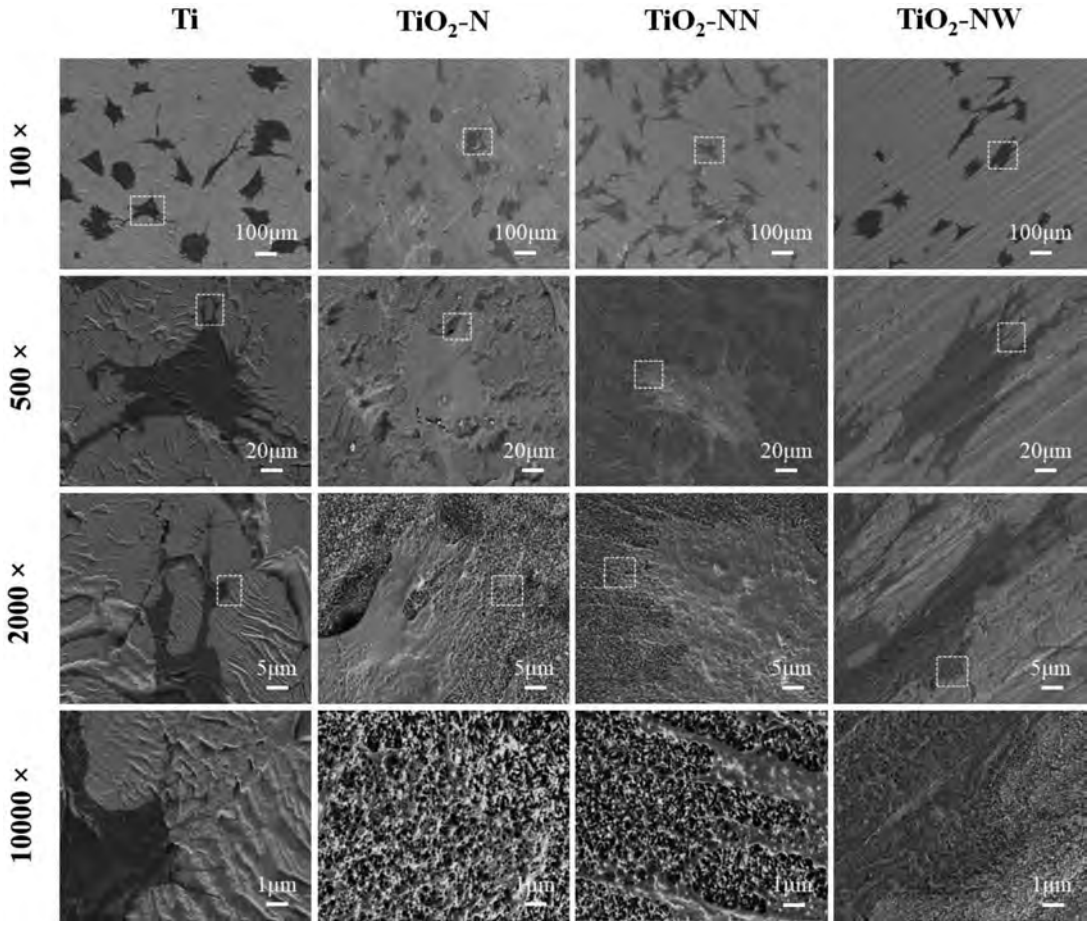

Fig. 5. Morphologies of the BMSCs cultured on the samples for 1 day. The high-magnification images are taken from the area surrounded by squares in the low-magnification images.

24 h, stimulated with LPS, and cultured in the serum-free normal medium for 12 h. The cells were fixed with 4% PFA and washed with PBS.

In the iNOS experiment, 1 mL of the immunostaining permeabilizer (Triton X-100) was added and permeabilized for 20 min and then the cells were rinsed with PBS. 1 mL of the QuickBlock™ closure solution (PBS) was added and remained for 1 h. After the blocking solution was removed, 500 μL of the diluted primary antibody Anti-iNOS antibody (1:1000, Abcam, UK) was added and incubated for 1 h, then overnight at 4 °C. Next, after incubating for 1 h and washing with PBS, 300 μL of the diluted secondary antibody m-IgGk BP-CFL 555 (1:100, sc-516177, Santa Cruz Biotechnology, USA) was added and incubated for 1.5 h followed by washing with PBS. The nuclei were stained by DAPI for 5 min, washed with PBS, and photographed by CLSM. The CD206 uses the immunostaining permeabilizer (Saponin), primary antibody CD206 (1:2000, Abcam, UK) and secondary antibody m-IgGκ BP-CFL 488 (1:100, sc-516176, Santa Cruz Biotechnology, USA).

2.7. Statistical analysis

The experiments were repeated 3 times and the data were shown as mean ± standard deviation (SD) based on the statistical software SPSS 14.0. Statistical analysis was performed using one-way analysis of variance and Student-Newman-Keuls (SNK) post hoc test. $^{*}p < 0.05$, $^{**}p < 0.01$, and $^{***}p < 0.001$ were considered to be statistically significant, highly significant and extremely significant, respectively.

3. Results and discussion

3.1. Characterization

Various nanostructures were prepared on Ti hydrothermally. The nanorod structure was produced using a hydrothermal solvent containing NaOH and by increasing the reaction time, the nanoleaf structure morphs into a nanorod-like morphology. However, as the hydrothermal time is increased further, the nanorods become twisted and entwined with each other forming a disordered structure (Fig. S1 in Supplementary Information). A second process is thus adopted to adjust the diameter and morphology of the nanorods by changing the solvent in the hydrothermal treatment. TiO_2-N was fabricated on Ti by a one-step hydrothermal treatment in NaOH, whereas TiO_2-NN and TiO_2-NW were prepared using a second hydrothermal treatment with NaOH and deionized water, respectively. As shown in Fig. 2(a), the three TiO_2 nanostructures have uniform density and spatial distribution. The diameters of the nanorod on TiO_2-N, TiO_2-NN and TiO_2-NW are about 45, 60 and 32 nm, respectively. The spacing values of the nanostructures in each of these three groups are measured from the SEM images, and are about 42, 60 and 28 nm, respectively. AFM shows that the roughness of TiO_2-N, TiO_2-NN and TiO_2-NW is 129, 110, and 40.5 nm. After the secondary hydrothermal treatment, the roughness of the nanoarrays decreases. The three TiO_2 nanostructures are characterized by TEM (Fig. 2(c)). Nanorods with a diameter of about 45 nm are observed from the TiO_2-N group but that of the nanorods in the TiO_2-NN group is 60 nm. This further

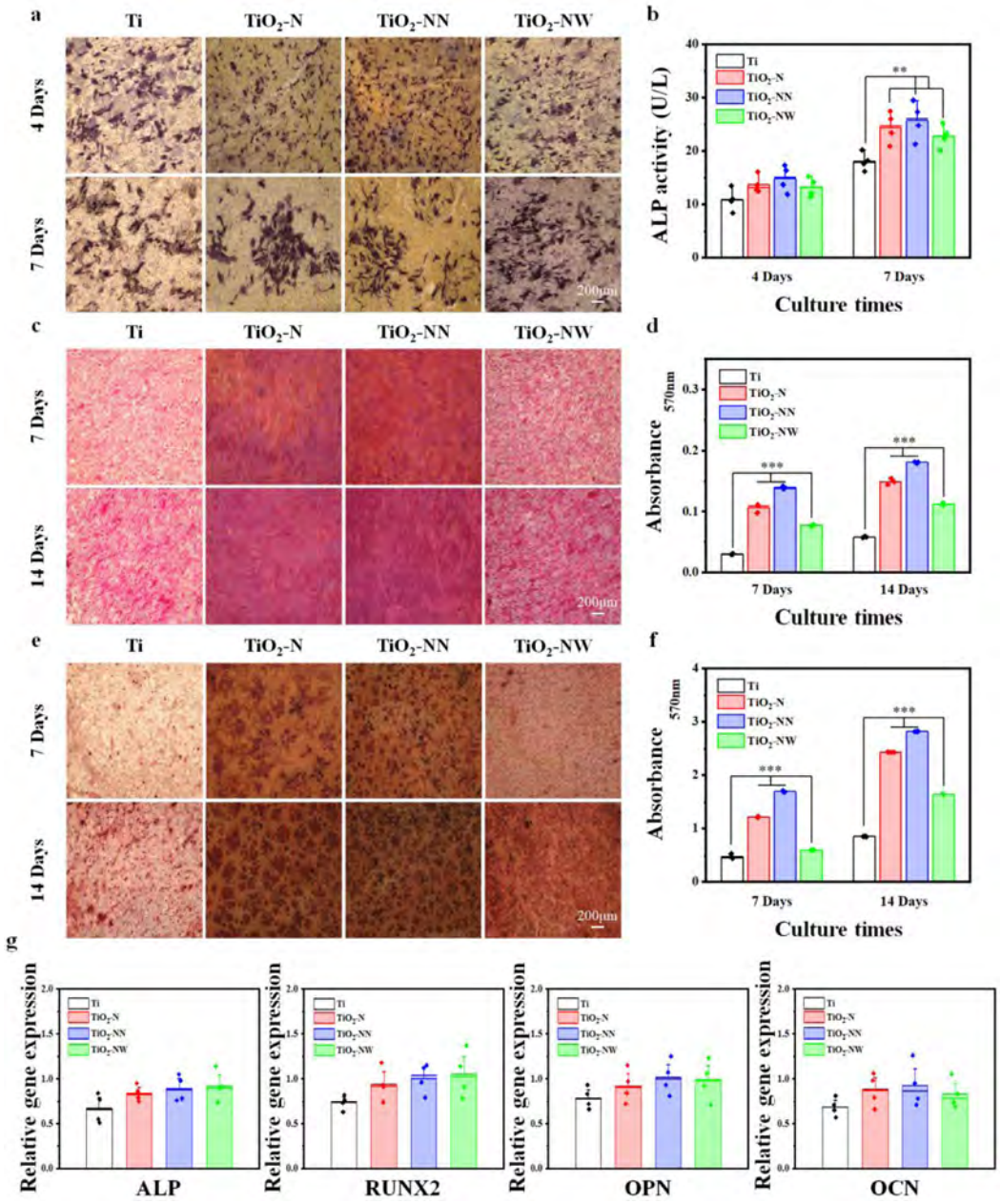

Fig. 6. Osteogenesis of BMSCs on the nanoarrays. (a, b) Qualitative images and quantitative results of the ALP activity of BMSCs after osteogenesis induction for 4 and 7 days. (c, d) Qualitative images and quantitative results of type I collagen secretion by the BMSCs after osteogenesis induction for 7 and 14 days. (e, f) Qualitative images and quantitative results of mineralization after osteogenesis induction for 7 and 14 days. (g) Effects of the nanoarrays on the osteogenesis-related genes ALP, RUNX2, OPN and OCN by RT-qPCR (** $p < 0.01$, *** $p < 0.001$).

confirms the successful preparation of nanoarrays on Ti. A lattice spacing of 0.35 nm is observed from the (101) plane of TiO_2 as shown in Fig. 2(c) [35,36] because the precipitation rate of TiO_2-N is larger than the dissolution rate in NaOH in the second hydrothermal step [27]. When the solvent in the second hydrothermal treatment is changed to deionized water, a nanocone structure is observed (TiO_2-NW) possibly because when the dissolution rate of TiO_2-N is higher than the precipitation rate, highly anisotropic growth results. During the reaction in deionized water, growth occurs along the preferred direction leading to the formation of rod-shape structures with sharp facets. If the hydrothermal reaction proceeds, the nanocone structure forms gradually [40].

The chemical states of the TiO_2 nanoarrays are determined by XPS (Fig. 3(a)) and the high-resolution spectra of Ti and O confirm the formation of TiO_2. Fig. 3(b) shows the XRD patterns of Ti and TiO_2 nanoarrays. The nanoarrays are mainly composed of anatase TiO_2 and Ti. The surface wettability is shown in Fig. 3(c). The contact angle on Ti is about 53° and decreases to about 13° on the TiO_2 nanoarrays, indicating that the TiO_2 nanoarrays improve the hydrophilicity of Ti. However, no significant difference is observed among the TiO_2-N, TiO_2-NN, and TiO_2-NW groups.

Protein adsorption is an essential step in the initial stage of cell adhesion and affects the subsequent interactions with cells [41]. The amounts of proteins adsorbing on the TiO_2 nanoarrays are presented in Fig. 3(d). The protein concentrations on TiO_2-N, TiO_2-NN, and TiO_2-NW are 0.231, 0.285, and 0.231 mg/mL, respectively, which are higher than that on Ti (0.208 mg/mL). This may be due to the improved hydrophilicity and special nanostructures [42]. The

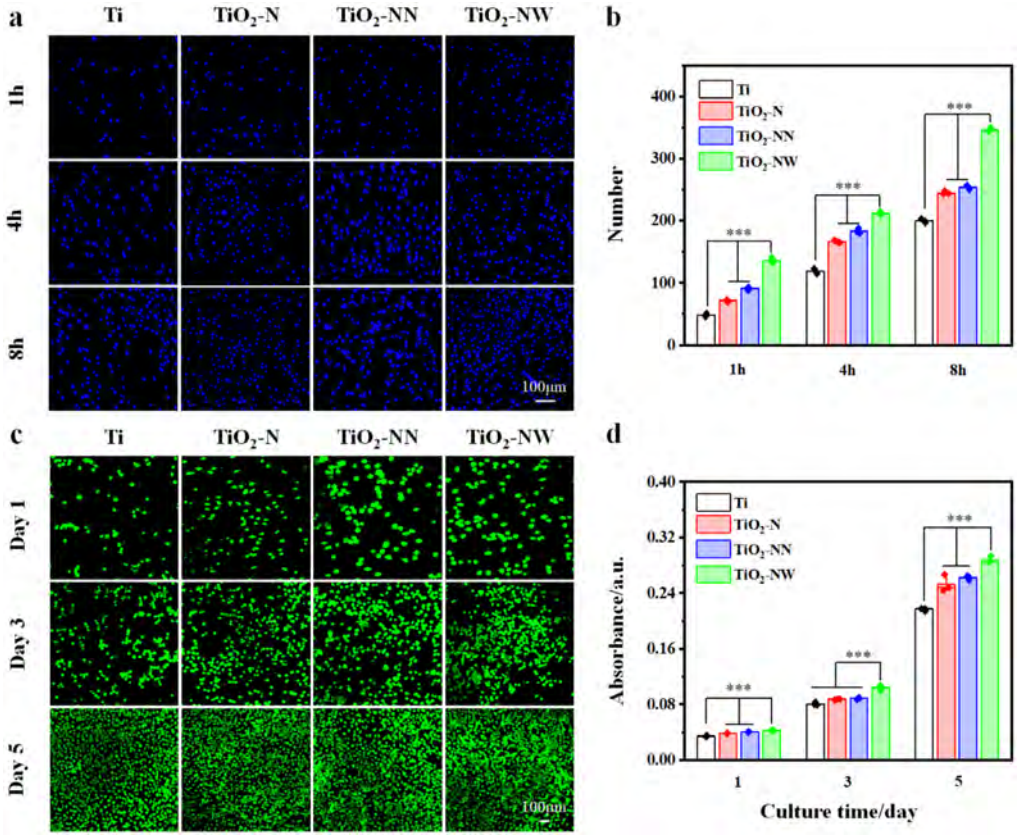

Fig. 7. Effects of the surface nanoarrays on osteoblasts. (a, b) CLSM images of the cell nuclei and quantitative results after culturing for 1, 4, and 8 h on Ti, TiO_2-N, TiO_2-NN, and TiO_2-NW. (c) CLSM images after live/dead staining of the osteoblasts after culturing for 1, 3, and 5 days. (d) MTT results after culturing for 1, 3, and 5 days (***$p < 0.001$).

corrosion resistance of Ti and TiO_2 nanoarrays is shown in Fig. S2 and the corresponding values of E_{corr} and I_{corr} obtained from the polarization curves are shown in Table S1 in Supplementary Information. The results show that the corrosion resistance of the samples with nanoarrays is better.

3.2. Effects of the nanoarrays on osteogenesis

The surface nanomorphology of implants affects protein adsorption and can stimulate osteoblast migration to accelerate osseointegration [43–45]. BMSCs have been shown to influence bone regeneration and benefit cellular therapy of bone diseases [46]. Herein, BMSCs are cultured on the nanoarrays to study the effects on osteogenesis.

The adhesion ability of BMSCs to the nanoarrays is assessed by DAPI staining. As shown in Fig. 4(a), after culturing for 8 h, the number of adherent cells on TiO_2-NN is larger than that on other samples. The cell morphology after culturing for 24 h is observed by FITC and DAPI staining (Fig. 4(b)). Compared to Ti, TiO_2-N, TiO_2-NN, and TiO_2-NW induce a higher F-actin assembly. In particular, spreading of BMSCs on TiO_2-NN and TiO_2-NW is better, especially on TiO_2-NN which reveals a polygonal shape with cellular pseudopodia. The results may be related to the roughness of the nanoarrays as the rougher TiO_2-NN promotes adhesion, diffusion, and differentiation of BMSCs [47]. Live/dead staining (Fig. 4(c)) and MTT assay (Fig. 4(d)) are performed to assess the cell viability and proliferation of BMSCs on the various nanoarrays. The metabolic activity of BMSCs on the nanoarrays is higher than that on Ti after culturing for 5 d showing the number of cells shows the order of TiO_2-NN> TiO_2-NW >TiO_2-N.

The SEM images of the BMSCs after incubation for 1 day are depicted in Fig. 5. BMSCs are observed to grow on all samples. Compared to Ti, flat lamellipodia are observed from TiO_2-N and TiO_2-NW and TiO_2-NN shows more pronounced stretching of the flattened plate-like feet. The nanostructures with improved roughness and hydrophilicity facilitate the adhesion of proteins, and the nanostructures provide more spacer sites for the adhering integrins [48,49], which changes the cellular behavior through cell-sensing morphology, thus presenting different orientations and shapes [50,51].

The ALP activity, collagen secretion, and ECM mineralization of the nanoarrays are determined to investigate osteogenic differentiation of BMSCs (Fig. 6). The qualitative micrographs and quantitative results disclose that the nanoarrays induce a higher amount of ALP than Ti. Among the different nanoarrays, the ALP activity of BMSCs on TiO_2-NN is the highest, followed by TiO_2-N and TiO_2-NW. Collagen secretion and ECM mineralization on the various nanoarrays are essentially the same as that of the ALP activity, confirming that TiO_2-NN facilitates osteogenic differentiation of BMSCs.

The effects of the nanoarrays on the expression of osteogenic-related genes are monitored from the gene perspective by RT-qPCR (Fig. 6(g)). Compared with Ti, all the nanoarrays upregulate the expressions of ALP, RUNX2, OPN and OCN. According to the early differentiation marker ALP and late differentiation marker OCN, the gene expression of TiO_2-N and TiO_2-NN is stronger than that of TiO_2-NW, especially TiO_2-NN. RUNX2 is an important upstream osteoblast-specific transcription factor [10,52] that stimulates transcription of osteogenesis-related genes such as ALP [53] and OCN [54] by combining specific regions. It has been shown that the development of the osteoblast phenotype requires a regulated interrelationship between proliferation and differentiation [11]. The expression of genes for ALP, RUNX2, OPN and OCN markers are all

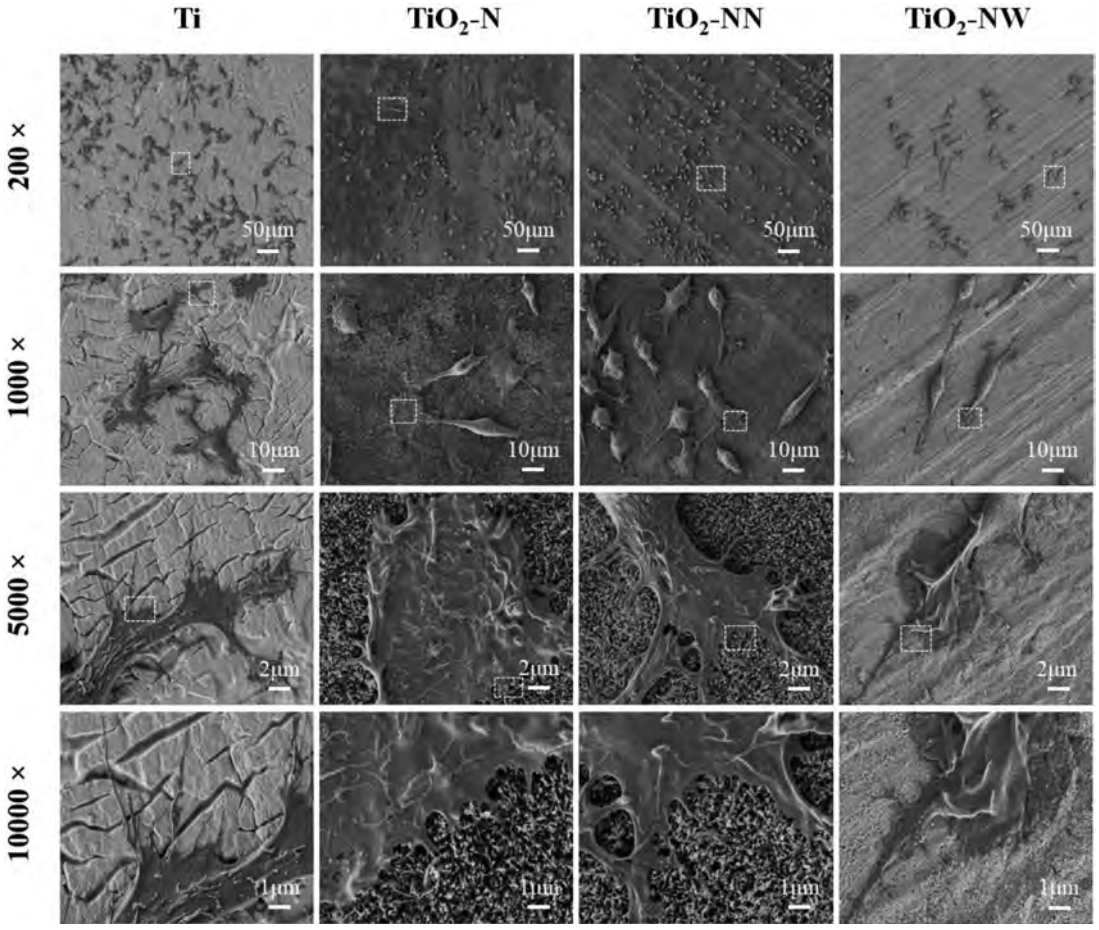

Fig. 8. FE-SEM images of the macrophages after incubation for 24 h on the samples and stimulation with LPS for 6 h. The high-magnification images are taken from the area surrounded by squares in the low-magnification images.

enhanced, but do not reach a statistical difference, probably because at this point cell proliferation reached its endpoint and osteogenic differentiation was underway [55].

The nanorods on TiO_2-NN show better adhesion, spreading, proliferation, and osteogenic differentiation of BMSCs boding well for the osteogenic capacity. Generally, the cell behavior on the surface of implants is influenced by many factors such as chemical composition, surface topography, hydrophilicity, and protein adsorption. As shown by our experiments, most of the nanoarrays are TiO_2 which possesses excellent biocompatibility. However, TiO_2 alone cannot regulate the cell behavior. It has been reported that a hydrophilic surface favors cell adhesion and proliferation [56], whereas a rough surface provides more sites for adherence of integrin clusters [49]. Accordingly, the nanoarrays favor growth and osteogenic differentiation of BMSCs due to the improved hydrophilicity and higher roughness [57]. The nanostructures also affect protein adsorption as well as integrin ligation and clustering [41], which further influence assembly of focal adhesion and alter the signaling pathways [58–60], then regulate cell shape and adhesion, and thus guide cell fate [61,62]. It has been shown that nanorods with a spacing value of about 70 nm can effectively promote cell proliferation, differentiation and osteogenesis [18,63], which is consistent with our results. TiO_2-NN adsorbs more protein under the same conditions because of the special surface nanostructure and furthermore, the diameter and spacing of the nanorods are more suitable for integrin activation and clustering. TiO_2-NN shows the best results in promoting adhesion, spreading, proliferation, as well as osteogenic differentiation of BMSCs.

3.3. Effects of the nanoarrays on osteoblasts

Directing BMSCs towards osteoblasts rather than other cell types is crucial to bone tissue engineering [64]. Hence, the osteoblast cell line of MC3T3-E1 is cultured on Ti and TiO_2 nanoarrays to study the effects. The cell morphology is observed by fluorescent staining (Fig. S3) and the high-magnification micrograph is shown in Fig. S4. Similar to the results of BMSCs, after incubation for 24 h, spreading of osteoblasts on all the nanoarrays is better than that on Ti. Among the different nanoarrays, TiO_2-NW induces more F-actin assembly than TiO_2-N and TiO_2-NN, and the cells on TiO_2-NW have a polygonal shape with filamentous and lamellar pseudopods. The results are inconsistent with those observed from the BMSCs. The initial adhesion, cell viability, and proliferation of osteoblasts are studied (Fig. 7) and all the nanoarrays promote better adhesion and proliferation of cells than Ti and the cell viability and numbers show the following order of TiO_2-NW $>TiO_2$-NN$>TiO_2$-N.

Osteoblasts exhibit different behavior on the TiO_2 nanoarrays compared to BMSCs. The osteoblasts are more sensitive to TiO_2-NW rather than TiO_2-NN probably due to the cell membrane characteristics and cell dimensions [65,66]. In terms of cell proliferation and cell viability, it has been shown that osteoblasts are less sensitive to nanogrooves than BMSCs [67]. It can be seen from Fig. 2(a) that TiO_2-NW nanogrooves are the shallowest, so TiO_2-NW is conducive to the adhesion and spreading of osteoblasts. Furthermore, it has been proved that osteogenic differentiation of BMSCs cultured on the nanosurface at Ra=110 nm was increased compared

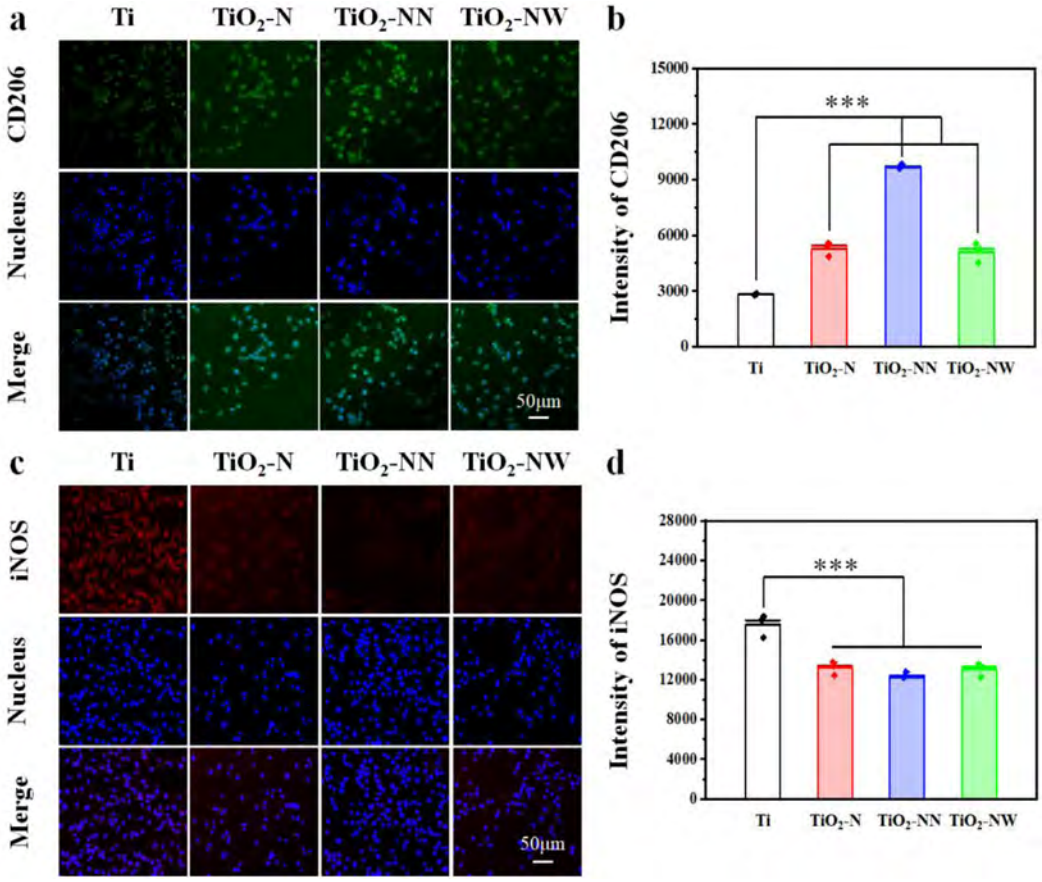

Fig. 9. Immunomodulatory effects of the surface nanoarrays on macrophages. (a) Fluorescence images of CD206 (green) and nuclei (blue). (b) Quantitative fluorescence intensities of macrophages on Ti, TiO_2-N, TiO_2-NN, and TiO_2-NW. (c) Fluorescence images of iNOS (red) and nuclei (blue). (d) Quantitative fluorescence intensities of macrophages on Ti, TiO_2-N, TiO_2-NN, and TiO_2-NW (***$p < 0.001$).

to Ra=49 nm [68–70]. Combined with the AFM results, it can be shown that TiO_2-NN is more favorable for the osteogenic differentiation of BMSCs. As discussed above, the cell behavior is related to many factors and different cells respond differently to the same factor. Osseointegration is a complex process involving osteogenesis, angiogenesis, osteoimmunomodulation, and so on [71,72] and several kinds of cells are frequently involved and so more studies are needed to illustrate the definitive effects of nanostructures on different types of cells.

3.4. Effects of the nanoarrays on the immune response

Macrophages are an important component of innate immunity and the functions can be modulated by the nano-textured topographies of implants [73]. After implantation, the immune response of macrophages to osseointegration depends on the implant surface and subsequently determines the fate of the implants [74–76]. In this study, macrophages are cultured on the samples to investigate the relationship between the nanoarrays and macrophage-induced bone immunomodulation.

The shape of macrophages is related to the phenotype. The M1 macrophages are usually round with invasive footprints and M2 macrophages are mainly elongated with a spindle shape with a lamellar footprint [77,78]. Macrophages are stimulated with LPS and the morphology of the macrophages is displayed in Fig. 8. Macrophages can grow on all the samples. However, the morphology of the macrophages on Ti is round, whereas the macrophages on the nanoarrays have a spindle shape and are extended in sheets. Moreover, there are more filamentous feet at the lamellar extension of the macrophages on TiO_2-NN. The surface morphology and hydrophilicity of implants affect the phenotype, spreading and morphology of macrophages [79,80], which are regulated by cell-material interactions [81–84]. In this work, we believe the specific nanorod with a larger diameter plays a major role in immunomodulation.

In order to further study the regulatory effects of the various nanoarrays on the phenotypic transformation of macrophages, the expression levels of protein of CD206 (CD206, as a representative M2 marker) and iNOS (iNOS, as a representative M1 marker) of the macrophages after culturing for 24 h are examined by fluorescence staining (Fig. 9). According to the qualitative images and quantitative results, all the nanoarrays enhance secretion of CD206 and downregulate secretion of iNOS from the macrophages. In particular, TiO_2-NN shows improved expression of the M2 marker but smaller expression of the M1 marker. The immunomodulatory effects of both TiO_2-N and TiO_2-NW are weaker than that of TiO_2-NN, and there is little difference in the expressions of CD206 and iNOS between the two. In addition, since LPS facilitates activation of macrophages towards the M1 type [43,85,86], the immunofluorescence photograph and quantitative results of the samples not stimulated with LPS are used to serve as a control group as shown in Fig. S5. Compared to LPS stimulation, secretion of CD206 increases but secretion of iNOS decreases in line with our conclusion. Based on the quantitative and qualitative results of immunofluorescence, it is evident that TiO_2-NN is more favorable for macrophage polarization toward the M2 type. Macrophages cultured on TiO_2-NN for 24 h might reduce macrophage secretion of inflammatory factors [77,87], inducing macrophage polarization to-

ward M2 type and release of anti-inflammatory cytokines. M2 type macrophages normally trigger extracellular matrix synthesis, cell proliferation and tissue remodeling in the latter stage [88]. In addition to having anti-inflammatory capacity [89], the released anti-inflammatory cytokines can also enhance osteoblast differentiation [90], thereby accelerating bone formation [91,92] and healing [93].

The immune response of macrophages is influenced by the surface characteristics of the implants such as the morphology, roughness, and hydrophilicity [81,84]. In this study, the effects of the nanoarrays on the immunomodulatory is similar with those of BMSCs. TiO_2-NN promotes macrophages towards the M2 phenotype, enhances secretion of CD206, and downregulates secretion of iNOS, suggesting that the surface characteristics of TiO_2-NN is more important in triggering the immune response and inducing macrophage polarization towards the M2 type after implantation. The immune environment further affects osteogenesis and angiogenesis essential to subsequent bone tissue regeneration.

4. Conclusion

Nanoarrays with three different morphologies are prepared on Ti hydrothermally in different solvents to enhance the osteogenic properties. The nanoarrays exhibit enhanced cell adhesion, proliferation, differentiation, and immunomodulatory effects. In particular, TiO_2-NN shows the best results in promoting osteogenic differentiation of BMSCs and stimulating macrophage polarization towards the pro-healing M2 type to generate an immune microenvironment. TiO_2-NW is more effective in enhancing adhesion and proliferation of osteoblasts. The results provide insights and guidance for the design of bioactive orthopedic and dental implants.

Declaration of competing interest

The authors declare that they have no known competing financial interests or personal relationships that could have appeared to influence the work reported in this paper.

Acknowledgements

This work was financially supported by the National Natural Science Foundation of China (No. 52171240), the Postdoctoral Science Foundation of China (No. 2021M691992), the Major Projects in Research and Development of Shanxi (Projects of International Cooperation, No. 201803D421090), the City University of Hong Kong Donation Research Grant (No. DON-RMG 9229021), the Hong Kong PDFS-RGC Postdoctoral Fellowship Scheme (Nos. PDFS2122-1S08 and CityU 9061014), and the Hong Kong HMRF (Health and Medical Research Fund) (Nos. 2120972 and CityU 9211320).

Supplementary materials

Supplementary material associated with this article can be found, in the online version, at doi:10.1016/j.jmst.2022.12.023.

References

[1] Z. Geng, Z.Y. Li, Z.D. Cui, J. Wang, X.J. Yang, C.S. Liu, Nano Lett 20 (2020) 7716–7721.
[2] Z.Z. Zhao, S.Q. Ma, C.X. Wu, X.W. Li, X.Y. Ma, H. Hu, J. Wu, Y.L. Wang, Z.H. Liu, ACS Appl. Mater. Interfaces 13 (2021) 33981–33994.
[3] K. Yusa, O. Yamamoto, H. Takano, M. Fukuda, M. Iino, Sci. Rep. 6 (2016) 29462.
[4] K. Bedoya, M. Tarce, C.A.M. Benfatti, B. Henriques, M.T. Mathew, W. Teughels, J.C.M. Souza, J. Periodontal Res. 52 (2017) 946–954.
[5] V. Jokanović, M. Vilotijević, B. Jokanović, M. Jenko, I. Anžel, D. Stamenković, V. Lazic, R. Rudolf, Corros. Sci. 82 (2014) 180–190.
[6] G.F. Wang, J.H. Li, K.G. Lv, W.J. Zhang, X. Ding, G.Z. Yang, X.Y. Liu, X.Q. Jiang, Sci. Rep. 6 (2016) 31769.
[7] N. Jiang, Z.J. Guo, D. Sun, Y.B. Li, Y.T. Yang, C. Chen, L. Zhang, S.S. Zhu, ACS Nano 12 (2018) 7883–7891.
[8] H. Ananth, V. Kundapur, H.S. Mohammed, M. Anand, G.S. Amarnath, S. Mankar, Int. J. Biomed. Sci. 11 (2015) 113–120.
[9] N. Wang, H.Y. Li, W.L. Lü, J.H. Li, J.S. Wang, Z.T. Zhang, Y.R. Liu, Biomaterials 32 (2011) 6900–6911.
[10] Y.N. Zhang, K. Wang, Y. Song, E.P. Feng, K. Dong, Y. Han, T.L. Lu, Appl. Surf. Sci. 528 (2020) 147055.
[11] R.A. Gittens, T. McLachlan, R. Olivares-Navarrete, Y. Cai, S. Berner, R. Tannenbaum, Z. Schwartz, K.H. Sandhage, B.D. Boyan, Biomaterials 32 (2011) 3395–3403.
[12] A. Dehghanghadikolaei, B. Fotovvati, Materials 12 (2019) 1795.
[13] L. Bai, Z.B. Du, J.J. Du, W. Yao, J.M. Zhang, Z.M. Weng, S. Liu, Y. Zhao, Y.L. Liu, X.Y. Zhang, X.B. Huang, X.H. Yao, R. Crawford, R.Q. Hang, D. Huang, B. Tang, Y. Xiao, Biomaterials 162 (2018) 154–169.
[14] I. Bajpai, A. Rukini, K.-J. Jung, I.-H. Song, S. Kim, Mater. Technol. 32 (2017) 535–542.
[15] Y. Soyoung, L. Sujeong, I. Bajpai, K. Sukyoung, Biomater. Res. 19 (2015) 4.
[16] L.Z. Zhao, S.L. Mei, P.K. Chu, Y.M. Zhang, Z.F. Wu, Biomaterials 31 (2010) 5072–5082.
[17] Z. Yuan, P. Liu, Y. Liang, B. Tao, Y. He, Y. Hao, W. Yang, Y. Hu, K. Cai, J. Mater. Chem. B 6 (2018) 1359–1372.
[18] D.M. Yu, S. Guo, D. Yang, B. Li, Z. Guo, Y. Han, Chem. Eng. J. 426 (2021) 131187.
[19] X. Yuan, Y. Kang, J. Zuo, Y.N. Xie, L. Ma, X.L. Ren, Z.Y. Bian, Q.P. Wei, K.C. Zhou, X.Y. Wang, Z.M. Yu, PloS One 13 (2018) e0196366.
[20] W.E. Yang, H.H. Huang, Appl. Surf. Sci. 471 (2019) 1041–1052.
[21] R. Smeets, B. Stadlinger, F. Schwarz, B. Beck-Broichsitter, O. Jung, C. Precht, F. Kloss, A. Gröbe, M. Heiland, T. Ebker, Biomed. Res. Int. 2016 (2016) 6285620.
[22] R.K. Silverwood, P.G. Fairhurst, T. Sjöström, F. Welsh, Y. Sun, G. Li, B. Yu, P.S. Young, B. Su, R.M. Meek, M.J. Dalby, P.M. Tsimbouri, Adv. Healthc. Mater. 5 (2016) 947–955.
[23] Y.M. Su, S. Komasa, T. Sekino, H. Nishizaki, J. Okazaki, Mater. Sci. Eng. C 59 (2016) 617–623.
[24] I. Bajpai, I. Hidayat, I. Song, J. Lee, S. Kim, J. Biomater, Tissue Eng 5 (2015) 403–410.
[25] M. Lorenzetti, I. Dogša, T. Stošicki, D. Stopar, M. Kalin, S. Kobe, S.A. Novak, ACS Appl. Mater. Interfaces 7 (2015) 1644–1651.
[26] I. Junkar, M. Benčina, R. Zaplotnik, M. Mozetič, S. Sodin-Šemrl, K. Lakota, A. Iglič, Method for Treatment of Medical Metals and Their Alloys, E.U. 21159240 (2020) Patent, No.
[27] J. Vishnu, V.K. Manivasagam, V. Gopal, C.B. Garcia, P. Hameed, G. Manivasagam, T.J. Webster, Hydrothermal treatment of etched titanium: A potential surface nano-modification technique for enhanced biocompatibility, Nanomed-Nanotechnol. Biol. Med. 20 (2019) 102016.
[28] A.I.M. Greer, V. Goriainov, J. Kanczler, C.R.M. Black, L.A. Turner, R.M.D. Meek, K. Burgess, I. MacLaren, M.J. Dalby, R.O.C. Oreffo, N. Gadegaard, ACS Appl. Mater. Interfaces 12 (2020) 33541–33549.
[29] M.J.P. Biggs, R.G. Richards, M.J. Dalby, Nanomed-Nanotechnol. Biol. Med. 6 (2010) 619–633.
[30] Z. Chen, A. Bachhuka, F. Wei, X.S. Wang, G.Q. Liu, K. Vasilev, Y. Xiao, Nanoscale 9 (2017) 18129–18152.
[31] M.J. Dalby, N. Gadegaard, R.O.C. Oreffo, Nat. Mater. 13 (2014) 558–569.
[32] L.E. McNamara, T. Sjostrom, K.E.V. Burgess, J.J.W. Kim, E. Liu, S. Gordonov, P.V. Moghe, R.M.D. Meek, R.O.C. Oreffo, B. Su, M.J. Dalby, Biomaterials 32 (2011) 7403–7410.
[33] M.Y. Yao, S. Cheng, G.Q. Zhong, J.L. Zhou, H.W. Shao, L.M. Ma, C. Du, F. Peng, Y. Zhang, Bioact. Mater. 6 (2021) 2729–2741.
[34] L. Ma, G.C. Li, J. Lei, Y. Song, X.B. Feng, L. Tan, R.J. Luo, Z.W. Liao, Y.S. Shi, W.F. Zhang, ACS Nano 16 (2022) 415–430.
[35] X.Y. Zhang, G.N. Zhang, M.Z. Chai, X.H. Yao, W.Y. Chen, P.K. Chu, Bioact. Mater. 6 (2021) 12–25.
[36] G.N. Zhang, Y.Q. Yang, J. Shi, X.H. Yao, W.Y. Chen, X.Y. Wei, X.Y. Zhang, P.K. Chu, Biomaterials 269 (2021) 120634.
[37] G.N. Zhang, X.Y. Zhang, Y.Q. Yang, H.Y. Zhang, J. Shi, X.H. Yao, X.Y. Zhang, Adv. Mater. Interfaces 7 (2020) 1901706.
[38] G.N. Zhang, X.Y. Zhang, Y.Q. Yang, R.F. Chi, J. Shi, R.Q. Hang, X.B. Huang, X.H. Yao, P.K. Chu, X.Y. Zhang, Biomater. Sci. 8 (2020) 391–404.
[39] X.Y. Li, Y. Zhang, G.X. Qi, Cytotechnology 65 (2013) 323–334.
[40] V.V.D. Rani, K. Manzoor, D. Menon, N. Selvamurugan, S.V. Nair, Nanotechnology 20 (2009) 195101.
[41] Y.Z. Zhang, X.M. Liu, Z.Y. Li, S.L. Zhu, X.B. Yuan, Z.D. Cui, X.J. Yang, P.K. Chu, S.L. Wu, ACS Appl. Mater. Interfaces 10 (2017) 1266–1277.
[42] P.G. Coelho, R. Jimbo, N. Tovar, E.A. Bonfante, Dent. Mater. 31 (2015) 37–52.
[43] L. Bai, P.R. Chen, Y. Zhao, R.Y. Hang, X.H. Yao, B. Tang, C.S. Liu, Y. Xiao, R.Q. Hang, Biomaterials 278 (2021) 121162.
[44] J.C.M. Souza, M.B. Sordi, M. Kanazawa, S. Ravindran, B. Henriques, F.S. Silva, C. Aparicio, L.F. Cooper, Acta Biomater 94 (2019) 112–131.
[45] N. Wang, H.Y. Li, W.L. Lu, J.H. Li, J.S. Wang, Z.T. Zhang, Y.R. Liu, Biomaterials 32 (2011) 6900–6911.
[46] X.Y. Chen, K.Y. Cai, M. Lai, L. Zhao, L.L. Tang, Adv. Eng. Mater. 14 (2011) B216–B223.
[47] S. Okada, H. Ito, A. Nagai, J. Komotori, H. Imai, Acta Biomater 6 (2010) 591–597.
[48] L.Le Guehennec, A. Soueidan, P. Layrolle, Y. Amouriq, Dent. Mater. 23 (2007) 844–854.
[49] J. Kiang, N. Sniadecki, A.J. Engler, Biophys. J. 102 (2011) 705a.
[50] C.S. Kim, J.H. Kim, B. Kim, Y.S. Park, H.K. Kim, H.T. Tran, S.H. Kim, H. Jeon, S. Kim, J.H. Sim, H.M. Shin, G. Kim, Y.J. Baik, K.-J. Lee, H.-Y. Kim, T.J. Yun, Y.S. Kim, H.-R. Kim, Adv. Funct. Mater. 27 (2017) 1703569.

[51] L. Yang, Z. Gong, Y. Lin, V. Chinthapenta, Q. Li, T.J. Webster, B.W. Sheldon, Adv. Funct. Mater. 27 (2017) 1702689.
[52] M. Cheng, Y. Qiao, Q. Wang, G. Jin, H. Qin, Y. Zhao, X. Peng, X. Zhang, X. Liu, ACS Appl. Mater. Interfaces 7 (2015) 13053–13061.
[53] W.G. Jang, E.J. Kim, I.-.H. Bae, K.-.N. Lee, Y.D. Kim, D.-.K. Kim, S.-.H. Kim, C.-.H. Lee, R.T. Franceschi, H.-.S. Choi, J.-.T. Koh, Bone 48 (2011) 885–893.
[54] J.W. Wei, J. Shimazu, M.P. Makinistoglu, A. Maurizi, D. Kajimura, H.H. Zong, T. Takarada, T. Iezaki, J.E. Pessin, E. Hinoi, G. Karsenty, Cell 161 (2015) 1576–1591.
[55] G.S. Stein, J.B. Lian, J.L. Stein, A.J. Van Wijnen, M. Montecino, Physiol. Rev. 76 (1996) 593–629.
[56] R. Zhou, D.Q. Wei, S. Cheng, W. Feng, Q. Du, H.Y. Yang, B.Q. Li, Y.M. Wang, D.C. Jia, Y. Zhou, ACS Appl. Mater. Interfaces 6 (2014) 4797–4811.
[57] J. Lee, B.S. Kang, B. Hicks, T.F. Chancellor Jr, B.H. Chu, H.-.T. Wang, B.G. Keselowsky, F. Ren, T.P. Lele, Biomaterials 29 (2008) 3743–3749.
[58] X. Liu, S. Wang, Chem. Soc. Rev. 43 (2014) 2385–2401.
[59] L. Richert, F. Vetrone, J.H. Yi, S.F. Zalzal, J.D. Wuest, F. Rosei, A. Nanci, Adv. Mater. 20 (2008) 1488–1492.
[60] R.A. Gittens, R. Olivares-Navarrete, Z. Schwartz, B.D. Boyan, Acta Biomater 10 (2014) 3363–3371.
[61] Y. Hou, L. Yu, W. Xie, L.C. Camacho, M. Zhang, Z. Chu, Q. Wei, R. Haag, Nano Lett 20 (2020) 748–757.
[62] J.H. Zhou, B. Li, Y. Han, L.Z. Zhao, Nanomed-Nanotechnol. Biol. Med. 12 (2016) 1161–1173.
[63] D.M. Yu, S. Guo, M. Yu, W.W. Liu, X.K. Li, D.F. Chen, B. Li, Z. Guo, Y. Han, Bioact. Mater. 10 (2022) 323–334.
[64] W.Y. Qian, L.Q. Gong, X. Cui, Z.J. Zhang, A. Bajpai, C. Liu, A.B. Castillo, J.C.M. Teo, W.Q. Chen, ACS Appl. Mater. Interfaces 9 (2017) 41794–41806.
[65] V.V.D. Rani, L. Vinoth-Kumar, V.C. Anitha, K. Manzoor, M. Deepthy, V.N. Shantikumar, Acta Biomater 8 (2012) 1976–1989.
[66] C.C. Yin, Y.J. Zhang, Q. Cai, B.S. Li, H. Yang, H.L. Wang, H. Qi, Y.M. Zhou, W.Y. Meng, J. Biomed. Mater. Res. A 105 (2017) 757–769.
[67] R.A. Gittens, R. Olivares-Navarrete, T. McLachlan, Y. Cai, S.L. Hyzy, J.M. Schneider, Z. Schwartz, K.H. Sandhage, B.D. Boyan, Biomaterials 33 (2012) 8986–8994.
[68] K. Takeuchi, L. Saruwatari, H.K. Nakamura, J.M. Yang, T. Ogawa, J. Biomed. Mater. Res. A 72A (2005) 296–305.
[69] P.T. de Oliveira, A. Nanci, Biomaterials 25 (2004) 403–413.
[70] P.T. de Oliveira, S.F. Zalzal, M.M. Beloti, A.L. Rosa, A. Nanci, J. Biomed. Mater. Res. A 80A (2007) 554–564.
[71] B. Li, P. Gao, H.Q. Zhang, Z. Guo, Y.F. Zheng, Y. Han, Biomater. Sci. 6 (2018) 3202–3218.
[72] J.E. Davies, V.C. Mendes, J.C.H. Ko, E. Ajami, Biomaterials 35 (2014) 25–35.
[73] Z.T. Chen, A. Bachhuka, F. Wei, X.S. Wang, G.Q. Liu, K. Vasilev, Y. Xiao, Nanoscale 9 (2017) 18129–18152.
[74] C. Dou, N. Ding, C.R. Zhao, T.Y. Hou, F. Kang, Z. Cao, C. Liu, Y. Bai, Q.J. Dai, Q.Y. Ma, F. Luo, J.Z. Xu, S.W. Dong, J. Bone Miner Res. 33 (2018) 899–908.
[75] J.X. Bai, H.Y. Wang, H. Chen, G. Ge, M. Wang, A. Gao, L.P. Tong, Y.Z. Xu, H.L. Yang, G.Q. Pan, P.K. Chu, D.C. Geng, Biomaterials 255 (2020) 120197.
[76] Z.Z. Wang, Y.M. Niu, X.J. Tian, N. Yu, X.Y. Yin, Z. Xing, Y.R. Li, L. Dong, C.M. Wang, Adv. Funct. Mater. 31 (2021) 2007408.
[77] H.W. Yang, M. Yu, R. Wang, B. Li, X. Zhao, Y.L. Hao, Z. Guo, Y. Han, Acta Biomater 116 (2020) 400–414.
[78] F.Y. McWhorter, T.T. Wang, P. Nguyen, T. Chung, W.F. Liu, Proc. Natl. Acad. Sci. U. S. A. 110 (2013) 17253–17258.
[79] J.O. Abaricia, A.H. Shah, M. Chaubal, K.M. Hotchkiss, R. Olivares-Navarrete, Biomaterials 243 (2020) 119920.
[80] J.O. Abaricia, A.H. Shah, M.N. Ruzga, R. Olivares-Navarrete, Clin. Oral Implants Res. 32 (2021) 487–497.
[81] Y.Z. Zhu, H. Liang, X.M. Liu, J. Wu, C. Yang, T.M. Wong, K.Y.H. Kwan, K.M.C. Cheung, S.L. Wu, K.W.K. Yeung, Sci. Adv. 7 (2021) eabf6654.
[82] N. Kartikasari, M. Yamada, J. Watanabe, W. Tiskratok, X.D. He, Y. Kamano, H. Egusa, Acta Biomater 137 (2022) 316–330.
[83] Y.D. He, Z. Li, X. Ding, B.Y. Xu, J.J. Wang, Y. Li, F.H. Chen, F.H. Meng, W. Song, Y.M. Zhang, Bioact. Mater. 8 (2022) 109–123.
[84] R.S.B. Lee, S.M. Hamlet, H.-.J. Moon, S. Ivanovski, Biomaterials 267 (2021) 120464.
[85] Y. Cheng, F.X. Bai, X.L. Ren, R.H. Sun, X.W. Guo, W. Liu, B. Wang, Y.H. Yang, X.L. Zhang, Y. Xu, C.Y. Li, X.Y. Yang, L.F. Gao, C.H. Ma, X.E. Li, X.H. Liang, Cancer Res 82 (2022) 1603–1616.
[86] K. Yang, J.J. Xu, M. Fan, F. Tu, X.H. Wang, T.Z. Ha, D.L. Williams, C.F. Li, Front. Immunol. 11 (2020) 587913.
[87] X.Y. Dai, Y. Wei, X.H. Zhang, S. Meng, X.J. Mo, X. Liu, X.L. Deng, L. Zhang, X.M. Deng, J. Nanomater. 2015 (2015) 1–8.
[88] D.M. Mosser, J.P. Edwards, Nat. Rev. Immunol. 10 (2010) 460.
[89] B.N. Brown, B.D. Ratner, S.B. Goodman, S. Amar, S.F. Badylak, Biomaterials 33 (2012) 3792–3802.
[90] J. Lee, H. Byun, S.K. Madhurakkat Perikamana, S. Lee, H. Shin, Adv. Healthcare Mater. 8 (2019) 1801106.
[91] D.O. Freytes, J.W. Kang, I. Marcos-Campos, G. Vunjak-Novakovic, J. Cell Biochem. 114 (2013) 220–229.
[92] N. Mokarram, R.V. Bellamkonda, Ann. Biomed. Eng. 42 (2014) 338–351.
[93] J.R. Alhamdi, T. Peng, I.M. Al-Naggar, K.L. Hawley, K.L. Spiller, L.T. Kuhn, Biomaterials 196 (2019) 90–99.

Supplementary Information

Regulation of TiO_2 nanoarrays on titanium implants for enhanced osteogenic activity and immunomodulation

Ruoyu Li [a], Hongyu Zhang [b], Xiaohong Yao [a], Bin Tang [a,*], Paul K Chu [c], Xiangyu Zhang [a,d,*]

[a] Shanxi Key Laboratory of Biomedical Metal Materials, College of Materials Science and Engineering, Taiyuan University of Technology, Taiyuan 030024, China

[b] Department of Occupational Diesease, Second Hospital of Shanxi Medical University, Taiyuan 030001, China

[c] Department of Physics, Department of Materials Science and Engineering, and Department of Biomedical Engineering, City University of Hong Kong, Tat Chee Avenue, Kowloon, Hong Kong, China

[d] College of Biomedical Engineering, Taiyuan University of Technology, Taiyuan 030024, China

[*]Corresponding authors.

E-mail addresses: zhangxiangyu@tyut.edu.cn (X.Y. Zhang); tangbin@tyut.edu.cn (B. Tang).

Supporting Figures

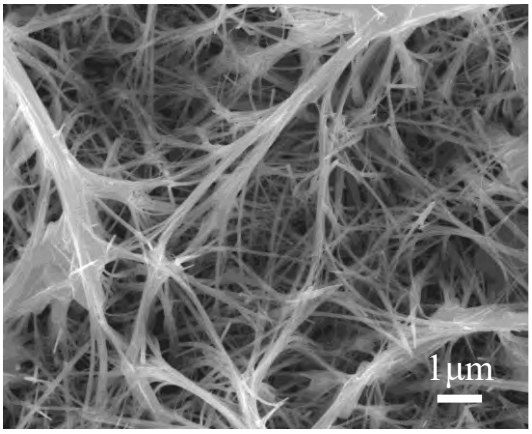

Fig. S1. SEM image of conducting a one-step hydrothermal treatment for 8 h.

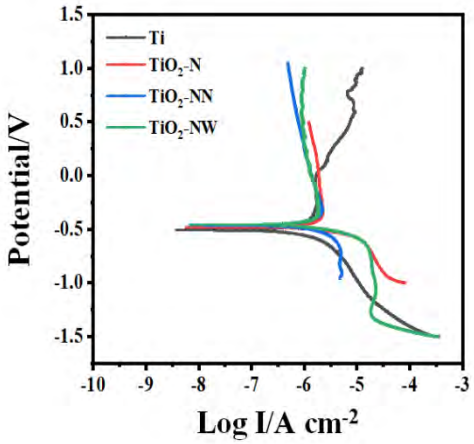

Fig. S2. Typical potentiodynamic polarization curves of Ti and TiO_2 nanoarrays in 0.9 wt.% NaCl solution.

Table S1 Electrochemical parameters obtained from potentiodynamic polarization curves of Ti and TiO_2 nanoarrays in 0.9 wt.% NaCl solution.

Sample	E_{corr} (V)	I_{corr} (A/cm^2)$\times 10^{-6}$
Ti	-0.508	7.828
TiO_2-N	-0.480	3.364
TiO_2-NN	-0.464	2.948
TiO_2-NW	-0.457	2.718

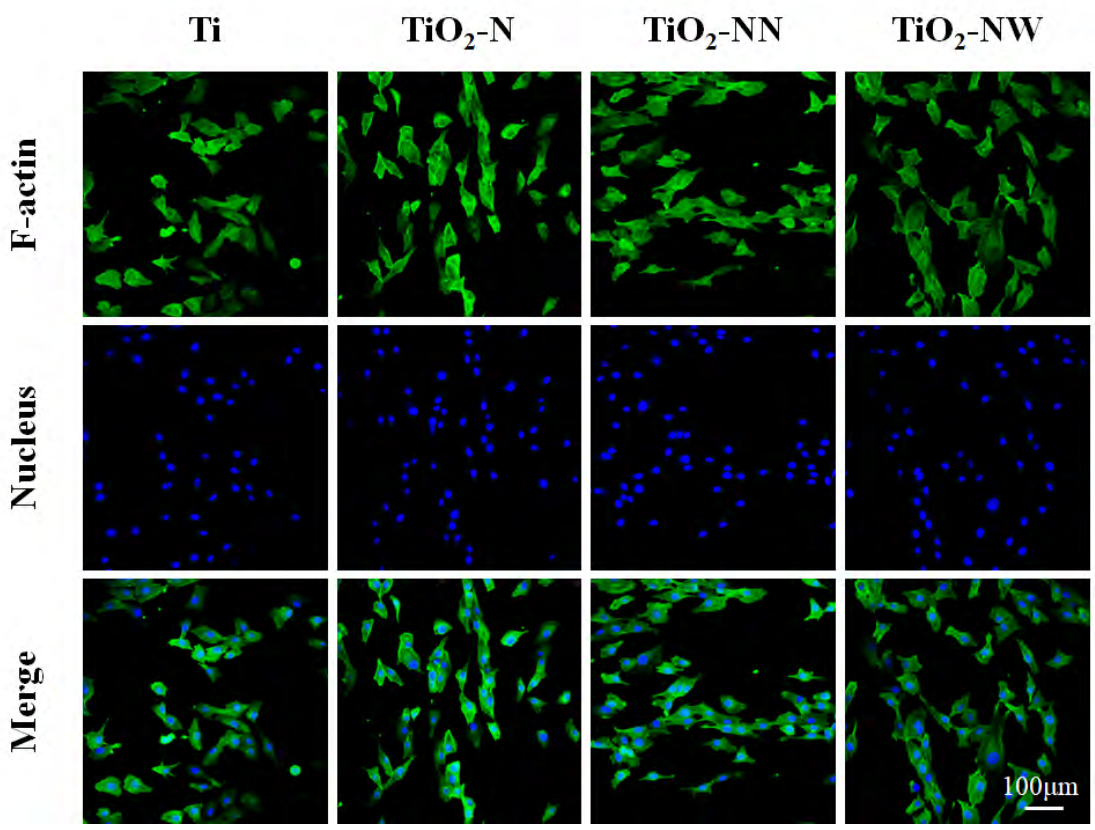

Fig. S3. Fluorescent images of the osteoblasts by CLSM with F-actin stained with FITC (green) and nucleus stained with DAPI (blue).

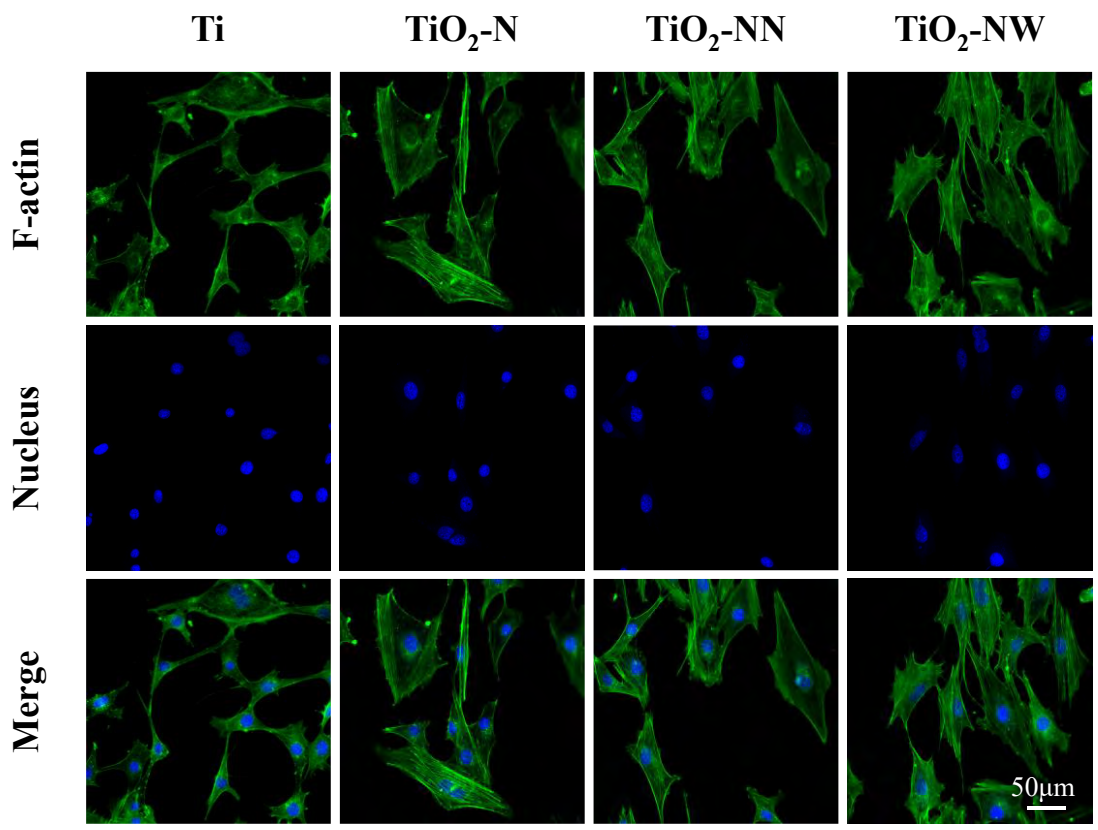

Fig. S4. High magnification cytoskeleton of osteoblasts. F-actin was stained with FITC (green) and nucleus was stained with DAPI (blue).

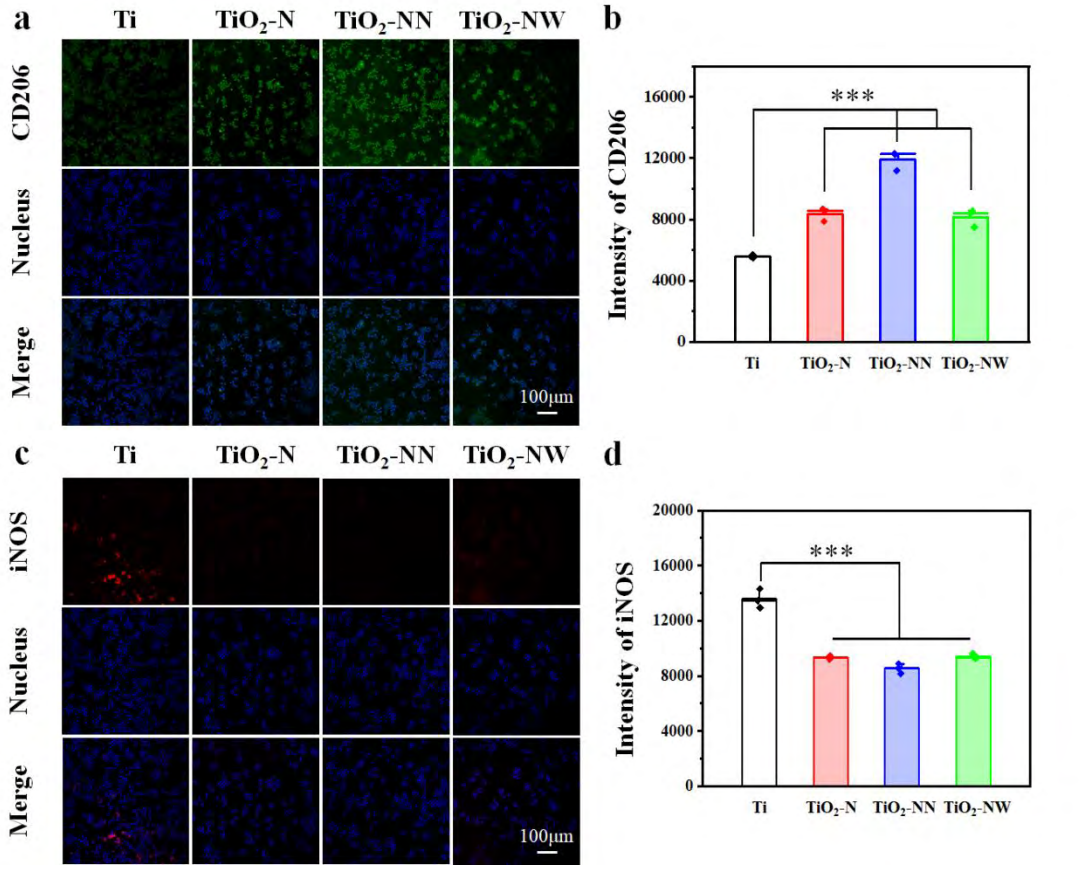

Fig. S5. Immunomodulatory effects of surface nanoarrays on macrophages. (a) Fluorescence staining images of CD206 (green) and nucleus (blue). (b) Quantitative fluorescence intensity values of macrophages on Ti, TiO_2-N, TiO_2-NN and TiO_2-NW. (c) Fluorescence staining images of iNOS (red) and nucleus (blue). (d) Quantitative fluorescence intensity values of macrophages on Ti, TiO_2-N, TiO_2-NN and TiO_2-NW (***P<0.001).